J Mater Sci: Mater Med (2008) 19:683–693
DOI 10.1007/s10856-007-3073-y

Performance of CF/PA12 composite femoral stems

Melissa Campbell · Martin N. Bureau · L'Hocine Yahia

Received: 19 September 2006 / Accepted: 2 April 2007 / Published online: 10 July 2007

Abstract This study presents the microstructural and mechanical behavior of the CF/PA12 composite material developed as well as its biomechanical performance when used for the fabrication of femoral stems. The static tests were performed to evaluate the compressive and flexural modulus as well as the ultimate compressive and bending strength. It was found that CF/PA12 composite had bone-matching properties in the same order of magnitude as cortical bone in the femur. Density and void content measurements were also done to assess the consolidation quality. Dynamic fatigue testing was conducted on both CF/PA12 cylinders and femoral stems to evaluate the long term durability and mechanical reliability of the composite. Compression–compression cyclic loading was used at a frequency of 6 Hz with loads varying between 17 kN and 22 kN for the composite cylinders while a frequency of 10 Hz and load of 2300 N was employed for the femoral stems. Results indicate that the fatigue performance of CF/PA12 composite surpasses by far the required fatigue performance for total hip prosthesis (THP) stems. The overall performance of the CF/PA12 femoral stems confirms that this composite is an excellent candidate material for orthopedic applications such as THP stems.

M. Campbell · L'HocineYahia
École Polytechnique de Montréal, Montreal, QC, Canada

M. N. Bureau (✉)
Industrial Materials Institute, National Research Council Canada, Montreal, QC, Canada
e-mail: martin.bureau@cnrc-nrc.gc.ca

Introduction

Primary total hip arthroplasty (THA) in the United States is estimated to grow by 174%, from 208,600 in 2005 to 572,100 in 2030 [1]. Recent studies have shown that this surgery is becoming more frequent in younger and more active patients, hence the need to increase the rate of survivorship of these implants. A few decades ago, stem breakage, gross acetabular wear or total fatigue failure of metallic femoral stems were considered as major causes of failure for THAs [2]. Nowadays, aseptic loosening, related to osteolysis of wear debris created at the articular joint and to micromotions at the bone-implant interface, is considered as the predominant cause of metallic hip implant revision. When revision surgeries are performed, bone resorption, related to the difference in rigidity between the implant and the host tissue (i.e., femur) is a concern since the host bone becomes weaker and less capable of receiving larger hip implants. This phenomenon is known as "stress shielding" and is frequently seen with metallic implants. In addition, this stress shielding might contribute to the stress concentration at the bone-implant interface that lead to micromotions, as recently indicated by a finite element simulation study of total hip prosthesis (THP) stems [3]. To date, it has not been demonstrated that stress shielding is not a factor in the prevalence of bone-implant interface weakening.

Despite the relative success of currently used metallic implants, evidence has shown that improved and more durable hip prostheses are still in demand. Because hip prostheses are submitted to complex and high mechanical loadings and to a corrosive environment, candidate materials other than metallic alloys are however very limited. The corrosion resistance, mechanical reliability and tailorability of thermoplastic polymer-based composites make

them a potential substitute for metallic materials, with a wider range of bone-matching properties. In fact employing advanced composite materials has become a common trend in the development of novel hip stems [4–11].

Previous studies on polymer composite materials designed for hip prostheses include the work from Reinhardt et al. [4], Simoes and Marques [5–7] as well as many other investigators [8–11]. Reinhardt et al. designed a thermosetting polymer-based composite hip prosthesis made by resin transfer molding (RTM). In this study, a new manufacturing technique was used to fabricate a hip prosthesis with stiffness similar to that of the surrounding bone. Even though, a certain similarity in mechanical properties with respect to bone was reached, further revisions were needed to improve the performance of the prosthesis and the fabrication process. Simoes et al. designed a composite hip femoral prosthesis with an internal Co–Cr core and a flexible composite outer layer. The prosthesis was manufactured using compression molding and results obtained show how adequate this material is to manufacture a controlled stiffness composite proximal femoral prosthesis. A composite hip prosthesis made from polyetherimide with carbon and glass fiber reinforcement was fabricated by De Santis et al. [9]. The effect of fiber organization on the mechanical properties was evaluated and results show that in tension, the strength and tensile modulus of the stem are respectively, 600 MPa and 40 GPa, while the flexural modulus in bending varies from 10 GPa to 60 GPa in the tip-head direction. Akay and Aslan [11] manufactured a short carbon fiber-reinforced polyetheretherketone (PEEK) prosthesis by injection molding and compared it with a titanium alloy (Ti–6Al–4V) prosthesis of the same geometry. Further studies were conducted concerning the clinical validity of composite stems. Adam et al. [10] conducted a human clinical study of a press-fit carbon fiber hip prosthesis with a smooth surface. The modulus of a carbon fiber-reinforced carbon stem is about three times lower compared with metal stems and closer to the modulus of cortical bone (ranging from 12GPa to 20 GPa). This study revealed that carbon fiber composite material has the mechanical properties to resist the physiologic stress of a hip joint, but that insufficient bone fixation due to the smooth surface of the prosthesis caused early loosening of the implant. From this survey of recent advancements in THPs, it is apparent that a biomimetic hip prosthesis with good bone fixation has not yet been developed.

To achieve this goal, a good understanding of bone's structure and properties in necessary. Bone forms the protective load-bearing skeletal framework of the body and it has an excellent capacity for self-repair. It is an anisotropic, heterogeneous material that is able to adapt to changes in mechanical usage patterns by remodeling, i.e., by density, porosity and thickness accordingly [12]. It is proposed here that, since the hip implant acts as a substitute for the femur, it must have similar mechanical properties. The mechanical properties of the femur, the longest bone in the human body composed for 80% of its mass of cortical bone (external dense and hard layer of the femur), are reported in Table 1.

Table 1 General mechanical characteristics of different materials and living tissues

Material/ Tissue	Density (g/ cm^3)	Modulus (GPa)	Ultimate strength (MPa)	Poisson's ratio
Cancellous bone	0.03–0.12	0.04–1.0	1.0–7.0	0.01–0.35
Cortical bone	1.6–2.0	12–20	150	0.28–0.45
Titanium alloys	4.4–4.7	105	780–1050	0.33
Stainless steel	7.9	210	230–1150	0.27–0.30

The objective of this study is to demonstrate the mechanical reliability of THP stems made of advanced composite materials, especially in long-term testing conditions reproducing physiological stress state. Specifically, carbon fiber-reinforced polymer composites with a cylindrical configuration will be tested in repeated compression testing (fatigue) in physiological and non-physiological (extreme) loading conditions and with a THP stem configuration in physiological conditions reproducing normal gait. The composite envisaged is polyamide 12 (PA12) with a carbon-fiber (CF) reinforcement. A recent investigation of the biocompatibility of this material showed good osteoblastic cell adhesion and no adverse cytotoxic response in the peri-prosthetic tissues [13].

The current paper presents a thorough analysis of the mechanical properties and an evaluation of the performance of this innovative biomimetic design for femoral stems made from a carbon-fiber reinforced polymer composite. Both short and long term mechanical testing of the hip stem will be discussed in detail during this work. Emphasis is however put on long term fatigue testing since the fatigue behavior of bone resembles composite materials. They exhibit a gradual loss of stiffness and strength throughout the cyclic loading due to fatigue damage accumulation [14]. Determining the fatigue properties of this composite is thus important to better understand its mechanical and physiological behavior as well as its response when used in orthopedic procedures such as total hip arthroplasty.

Materials and methods

Design concept and preparation

The novel THP stem consists of a hollow structure made of a 3-mm thick CF-reinforced polymer composite coated, in

the proximal region, by a thin crystalline hydroxyapatite layer that promotes bone growth and integration. The THP stem is typical of modular designs that are implanted by press-fitting into the contiguous bone without the use of an acrylic bone cement anchor. The stem is straight, follows the natural curve of the femoral bone, has an oval cross-section, and a shaft angle of 135° [3].

A PA12/CF reinforced composite in the form of braided sleeves of commingled fibers of PA12 and carbon was used in this study. Respective contents of composite in PA12 and CF were 68 and 32% (wt.). Theoretical density was 1.443 g/cm^3. Cylindrical PA12/CF specimens with a 22 mm diameter and a 3-mm wall thickness were molded for short and long-term testing. The prototype composite stems (3-mm thick wall) proposed in this study were fabricated using an inflatable bladder compression molding method. Six layers of braided sleeves were mounted on a bladder and placed in an in house designed and produced steel mold. The mold was then inserted in a heated press at 250°C, maintained for 5 min with an applied internal pressure of 480 kPa. These prototypes were tested in fatigue according to ISO recommendations for testing stemmed femoral components. An example of the final prototype is shown in Fig. 1.

Microstructural characterization methods

Cross sections along the length of the stem were cut, polished and observed under optical microscopy. The microscope was used to observe the quality of consolidation, evaluate the percentage of porosities apparent in the samples and approximate the fiber/matrix volume content. Samples were also taken at different locations along the stem in order to measure the change in density and void content. Density measurements were completed using Archimedes' water immersion method and void content was calculated using the following equation:

$$\text{Void } (\%) = \frac{\rho_t - \rho_i}{\rho_t} \times 100 \quad (1)$$

where ρ_t and ρ_i are the theoretical and measured densities respectively. The CF/PA12 composite has a theoretical density of 1.443 g/cm^3. Results reported are averages of three specimens.

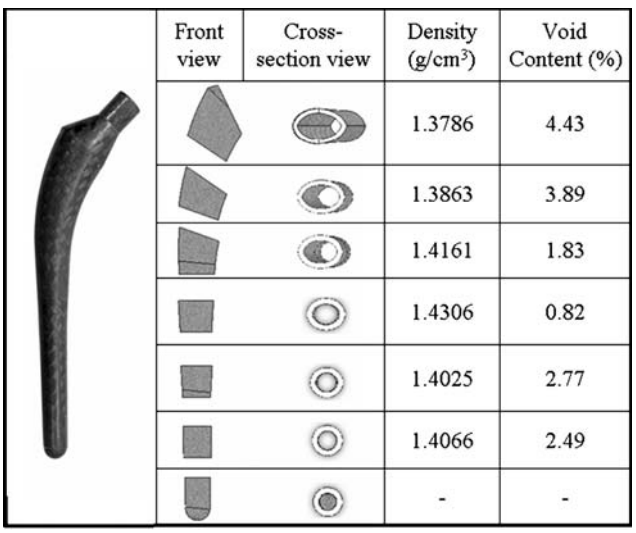

Fig. 1 CF/PA12 composite femoral stem

Mechanical testing method

Short-term mechanical tests (static testing)

Compression tests were carried out according to the general recommendations of ASTM D348–00 standard test method [15]. The static load tests were performed with an electromechanical Instron 5500R1125 tester with computer data acquisition. The compression specimens were carefully machined to 44 mm in length with parallel extremities. Uniaxial compression tests were done at room temperature with a crosshead speed of 5 mm/min and a 100 kN load cell. Parallel plates were utilized in order to help keep the composite cylinders leveled and ultimately prevent premature buckling. The compressive modulus of elasticity and ultimate compressive strength of the CF/PA12 composite cylinders were determined from the engineering curves. The standard deviation of the reported values is within 5%.

Flexural tests were executed according to ASTM D790M-03 [16] standard test method on flat specimens molded in the same conditions as the cylindrical specimens. This standard is designed for plastics but applies well to bone for three point bending tests and since our reference will be cortical bone throughout this study, tests were performed following this standard. The specimens were also carefully machined to a length of 100 mm and tested as recommended in ASTM D790M-03 with a span-to-thickness ratio of 32:1. The flexural tests were done at room temperature with a constant crosshead speed of 5 mm/min and a 25 KN load cell. The flexural modulus and strength of the CF/PA12 composite cylinders were determined from the load–deflection curves. Tests were ended when the first sign (cracks, fissures and/or breaks) of rupture was apparent.

Long-term tests (dynamic testing)

Cylindrical configuration: Cyclic fatigue testing was carried out on CF/PA12 composite cylindrical specimens

using an Instron 8874 axial-torsional table model fatigue system with a digital controller and computer-data acquisition. The geometry and setup of the specimen followed general recommendations from ASTM E2207-02 standard test method [17]. Tests were performed under load-controlled mode and using a sinusoidal waveform at 23°C and 50% R.H. Fatigue testing was done at room temperature under repeated (compression–compression) cyclic loading at a frequency of 6 Hz. The specimens were machined to a total length of 220 mm but the nominal gauge length of the fatigue specimens was 69 mm. Specimens tested were first inserted into metal cylinders in order to facilitate the grip on the composite tube and to prevent sliding once the test had begun, and then attached to the load frame using a three-jawed chuck.

In order to evaluate the mechanical durability of the composite, the specimens were subjected to four different levels of maximum stress loading of 95, 101, 112 and 123 MPa (17, 18, 20 and 22 kN), i.e. 50, 55, 60 and 70% of the pre-determined ultimate compressive strength. At least three specimens were tested for each fatigue load level. Cyclic fatigue testing ended when specimens showed a crack or sign of rupture. No magnifying device was used to observe the first sign of failure. When fatigue failure could not be obtained after 10×10^6 cycles or more for a specific set of conditions, an indefinite fatigue life was reported.

Computer-based data acquisition was employed to monitor and record the cyclic load versus position curves from which the progressive reduction of the compressive modulus at each fatigue cycle was obtained. Individual fatigue load-position loops, or hysteresis loops, were recorded for further data analysis using a logarithmic data sampling pattern. Evolution of the fatigue cycles as a function of the number of cycles could be monitored, as schematized in Fig. 2. The strain amplitude $\Delta\varepsilon/2$ was calculated for each sampled cycle from the displacement amplitude normalized by the specimen gage length to evaluate evolution of cyclic deformation during fatigue. The stiffness was obtained for each sampled cycle and normalized by the initial tangent slope to monitor specific stiffness evolution behavior. It was calculated as the tangent slope in the unloading section from the maximum compressive load point of the load—position loop. Despite the slightly higher than usually recommended cycling frequency, no significant hysteretic heating was noted during cyclic loading of all specimens, as monitored by K-type (nickel–chromium versus nickel–aluminum) thermocouples placed at the surface of the central section of the specimens. The fatigue results are also presented in the form of an S–N curve, i.e., the maximum cyclic stress and load versus the number of cycles to failure, from which the following Basquin's equation for each loading condition was obtained [18].

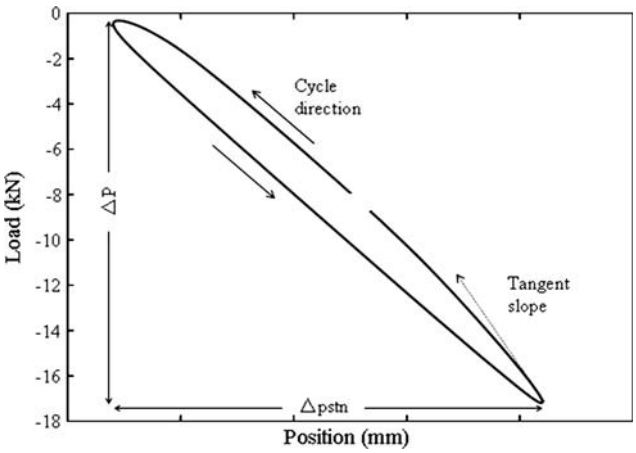

Fig. 2 Schematic drawing of hysteresis loops and measurements. P is considered as load and tangent slope is measured in second unloading part of cycle ($(\Delta\varepsilon/2 = \Delta p/2L)$,where ε is strain, p is position and L is gage length)

$$\sigma_a = \sigma'_f \times (2N_f)^b, \quad (2)$$

where σ_a is the fatigue stress amplitude, $\sigma'_f$is the fatigue strength coefficient, $2N_f$ is the number of cycles to failure and the exponent b is the fatigue strength exponent, a quantitative measure of the fatigue sensitivity. Fatigue specimens were also coated with a thin layer of platinum and then observed using a JEOL JSM-6100 scanning electron microscope (SEM) for fatigue damage observations.

THP stem configuration: In a second step, fatigue testing on the CF/PA12 hip stem was conducted on the same machine as the one used for the composite cylinders. Tests were performed according to the general recommendations of ISO 7206-4 [19] for the specimen and setup geometry and to ASTM F1612 [20] for the test procedure and report. The specimens had a total length of 230 ± 5 mm and were individually embedded in a polymer casting medium. The specimen was slowly lowered into the embedding medium (contained in a stainless steel rectangular mold called a specimen holder) until the center of the head was at a vertical distance of 130 mm from the embedding medium-free surface. The stem was held in position until completion of medium solidification. An urethane resin was used as an embedding medium and preliminary tests presented a modulus of elasticity of 3.5 GPa and a hardness of 28 HRC. Once the stem was anchored, it was then placed in a holder with an inclined platform that produced an out-of-plane moment and force on the prosthesis. The load was applied on the femoral head at an angle of $\beta = 11°$ and $\alpha = 0°$, as recommended in ISO 7206-4 for long anatomical stems. The test fixtures were constructed so that the load line passed through the center of the ball (femoral head). The loading apparatus incorporated a low-friction socket

applying the loads on the femoral head, as recommended in ISO 7206-4. The head of the prosthesis (hollow ball) was manufactured in house from stainless steel (316L) and inserted on the neck of the prosthesis. Tests were performed at 23°C and 50% R.H, with a sinusoidal waveform cycling at 10 Hz and with a load of 2,300 N. The same data acquisition was employed but data sampling was at a lower rate to reduce the number of data collected and a similar analysis of the results was done for the femoral stems. No significant hysteretic heating during cyclic loading was noted, as monitored by the same type of thermocouples as those used for the cylindrical configuration testing and an indefinite fatigue life was reported for specimens that exceeded 10×10^6 cycles. Results are reported as load–displacement curves.

Results and discussion

Microstructure

Micrographs of the cut and polished CF/PA12 composite stems are shown in Fig. 3. These images show that excellent consolidation quality and almost void-free samples were observed from the section between the proximal and distal part of the stem, whereas for the extremities (i.e., close to the neck and near the tip of the stem), small-sized voids and only fair consolidation quality was observed. Void content and density measurements at different locations of the molded stems are reported in Fig. 1. Low void contents (<2%) were obtained for samples from the mid-section of the stem. Slightly higher void contents (2–3%) were obtained for samples from the distal region of the stem. The highest void contents (3–4%) were obtained from the proximal region closest to the neck of the stem. More porosities and voids are visible at both extremities than in the central part of the stem, in agreement with micrographs in Fig. 3. These slight variations in microstructural characteristics along the length of the molded stems are attributed to the fabrication process of the femoral stem. These limited void contents of <2% to ≈4% are however comparable to typical void contents reported for processes used in long or continuous fiber-reinforced thermoplastic composites manufacturing, for which both static and fatigue behavior are close to optimal and only show slight variations in the void content range measured [21].

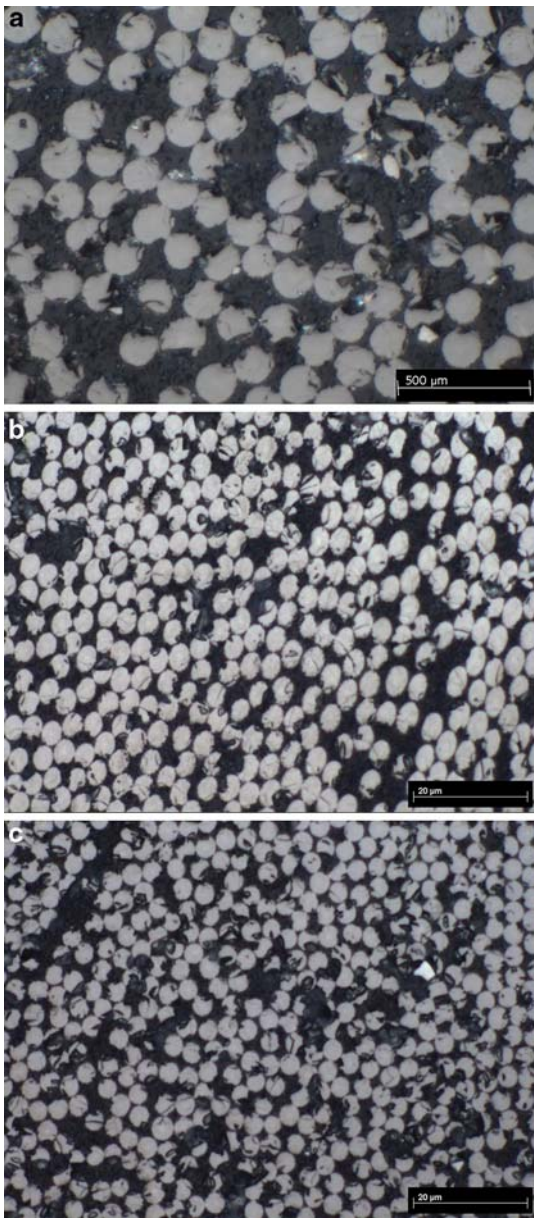

Fig. 3 Micrographs of samples taken from CF/PA12 femoral stems at various places along the stem's length: (**a**) proximal region near the neck of the stem with high void content (3–4%); (**b**) mid-section of the stem with low void content (<2%); (**c**) distal region of the stem with fairly high void content (2–3%). White spots in micrographs represent carbon fibers. Dark gray patches represent the polymer matrix and black spots indicate pockets of air

Mechanical properties

In this section, the mechanical properties of the CF/PA12 composite are compared to those of cortical bone. Since this composite is meant to be used for bone replacement and repair applications, in particular for a THP, the ultimate goal is to obtain a biomechanical performance similar to that of bone in order to prevent stress shielding and eventually bone resorption. All values for mechanical properties of cortical bone were taken from Wirtz et al. [22], Reilly et al. [23, 24] and Snyder and Schneider [25].

Static testing results

The compressive and flexural results of the CF/PA12 composites cylinders are reported in Table 2. Results in this table are compared to those of cortical bone found in the human femur. The calculated bending stiffness for the composite cylinders, based on the product of the modulus of elasticity and the moment of inertia, and reported bending stiffness for human cortical bone are also compared in Table 2. These results indicate that both the modulus and ultimate strength in flexural and compressive testing of CF/PA12 composite are either within or close to the reported range of properties of the femur. As expected from its design, the composite stem shows a bending stiffness ranging from 180 N m^2 to 425 N m^2 depending on stem diameter, very close to reported values of 170–500 N m^2 for human cortical femoral bone. Also, the composite cylinders, which had a nominal outer diameter (22 mm) and wall thickness (3 mm) comparable to the THP stems designed [3] failed at an absolute compressive maximum load of 28.6 kN. This load at failure is considerably above (close to three times) the maximum physiological load to which the femoral bone is subjected (10,000 N) when jumping on one leg [27], indicating the high level of performance expected from the composite THP stems. A comparison of the compressive modulus and strength values obtained from the CF/PA12 composite to those of cortical bone is presented in Table 2. They can be compared to those of commonly-used metallic materials for the fabrication of THP stems in Table 1. This comparison illustrates the advantages of fiber-reinforced polymer composites for replacing or substituting bone in place of metallic alloys showing very different properties.

Dynamic testing results

Fatigue of cylindrical specimens: Four different loading conditions were evaluated in fatigue and two different frequencies were used. The fatigue testing conditions are reported in Table 3. The maximum compressive loads range from 17 kN to 22 kN, respectively between 50% and 70% of the maximum load before rupture. These conditions are considerably more severe that the loading conditions in ASTM standard [27] for testing femoral stems recommending loading between 300 N and 3,000 N for a fatigue life of the femoral stem of at least 5 million cycles.

The S–N curves obtained are illustrated in Fig. 4 and reported in Table 3 both in terms of maximum fatigue stress and maximum fatigue load. As shown in Fig. 4 and Table 3, fatigue failures occurred after approximately 10^4 cycles for maximum fatigue load of 22 kN (i.e., 123 MPa), 10^5 cycles for maximum fatigue load of 20 kN (i.e., 112 MPa), 10^6 cycles for maximum fatigue load of 18 kN (i.e., 101 MPa) and close to 10^7 cycles and more for maximum fatigue load of 17 kN (i.e., 95 MPa). These results show fatigue life of 10^6 and more at load levels at least six times greater than load levels of 3,000 N recommended in ASTM standards [28], in agreement with the expected high level of performance from compressive load at failure.

Figure 5 illustrates the evolution of the hysteresis loops for two testing condition. This figure indicates that for a load level of 17 kN (Fig. 5a), showing fatigue life above 10^6 cycles, the surface, or opening, of the hysteresis loops progressively decreased as the number of cycles increased. This indicates that total cyclic deformation decreases during the fatigue life. A similar trend is noted for load levels of 18 kN. For load levels of 20 kN (Fig. 5b), for which fatigue life is approximately 10^5 cycles, the surface of the hysteresis loops did not appear to change as the number of cycles increased, indicating that total cyclic deformation was more or less constant throughout the fatigue test. A similar trend is noted for load levels of 22 kN, with the exception of the cycles close to fatigue failure which showed increasing hysteresis loop opening. The results thus indicate that for load levels of 20 kN and below, plastic deformation at each fatigue cycle was small, leading to fatigue endurance conditions, in which plastic defor-

Table 2 Mechanical results of the CF/PA12 composite (with human cortical bone values added for comparison)

Materials	Compressive			Flexural		Bending stiffness (N m^2)
	Maximum load (kN)	Modulus (GPa)	Ultimate strength (MPa)	Modulus (GPa)	Ultimate strength (MPa)	
CF/PA12 Composite	28.6 ± 3.8	12.2 ± 1.3	155 ± 27	16.4 ± 1.5	188 ± 15	180–425
Cortical bone	–	7.0–18.7[a]	175–265[a]	14.3–21.1[b]	178–250[b]	170–500[c]

[a] After [22]

[b] After [25]

[c] After [26], for outer cortex diameter of 25–30 mm; compared values for outer composite stem diameter of 20–25 mm

Table 3 Test conditions for compression fatigue testing (repeated cyclic loading) of CF/PA12 cylindrical tubes

Maximum load (kN)	Mean load (kN)	Maximum stress (MPa)	Cycles to failure	Decrease in strain amplitude[a] (mm/mm)	Constant strain amplitude rate[a] (/cycle)
17	–8.65	95	5,802,422	1.11×10^{-3}	-2.1×10^{-10}
			1,764,000		
			6,132,716		
			>10,272,465		
18	–9.15	101	1,328,721	9.1×10^{-4}	-8.2×10^{-10}
			1,262,408		
			930,070		
20	–10.15	112	221,788	8.5×10^{-4}	-8.70×10^{-9}
			122,117		
			158,160		
			803,642		
22	–11.15	123	9,015	4.4×10^{-4}	-2.247×10^{-7}
			4,332		
			13,658		

[a] During second phase shown in Fig. 8

mation is limited, characterized by extended fatigue life ($\geq 10^5$ cycles). However, for a load level of 22 kN, plastic deformation at each fatigue cycle was important, leading to rapidly increasing cumulative deformation, close to low-cycle fatigue conditions, and therefore fairly short fatigue life (10^4 and below).

Consistently with Fig. 5, Fig. 6 reports the relative stiffness of the composite specimens as function of the number of cycles for each fatigue load levels. As shown in Fig. 6, relative stiffness is reported from cycle 30, at which the load-position cycles became stable. The relative stiffness is thus calculated with the initial tangent slope on the unloading section of the hysteresis loops at cycle 30. For all load conditions, the relative stiffness increased as the

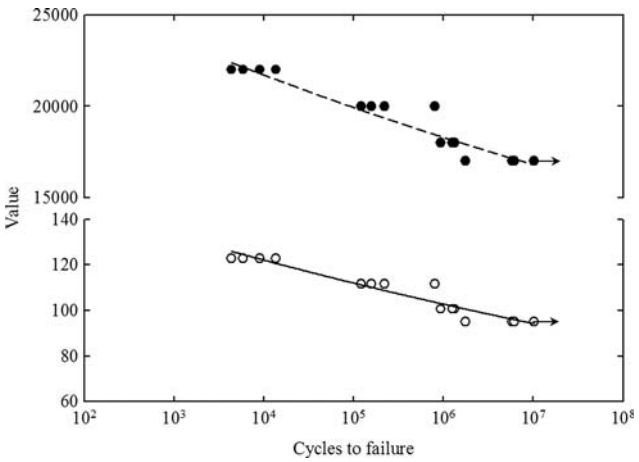

Fig. 4 Maximum cyclic stress in MPa (○) and maximum load in N (●) as a function of cycles to failure. Arrows indicate indefinite fatigue life

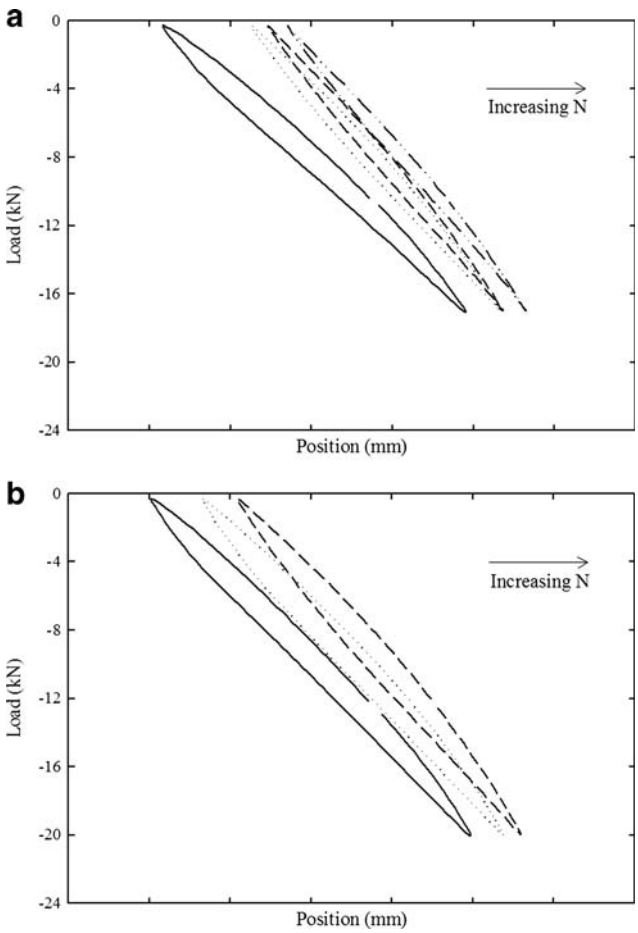

Fig. 5 Evolution of hysteresis loops for two different tested load conditions: (**a**) 17 kN (for cycle 30, 10^5, 10^6 and 5.5×10^6) and (**b**) 20 kN (for cycle 30, 5000 and 2×10^5)

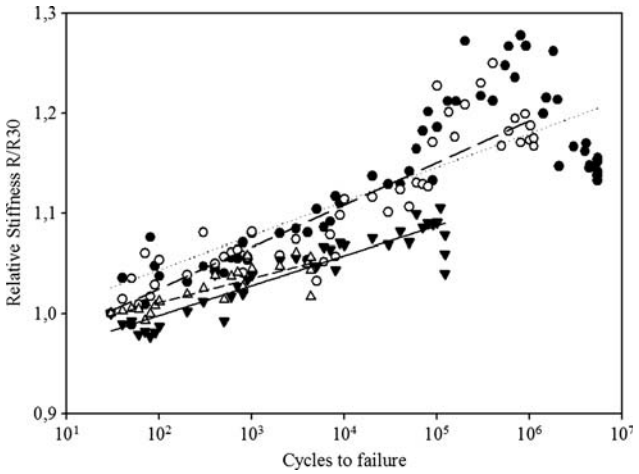

Fig. 6 Relative stiffness as a function of number of cycles to failure for 17 kN (●), 18 kN (○), 20 kN (▼) and 22 kN(△). Lines show linear regression for each tested condition

number of cycles increased. Towards the end of the tests (at high number of cycles), at least for load levels of 17 and 18 kN, the relative stiffness abruptly increased and then rapidly collapsed at the end of the tests. These results indicate that for most of the fatigue life, the fatigued specimen exhibited a behavior that resembles well known cyclic hardening in metallic alloys subjected to fatigue, since stiffness increased as cumulative deformation increased. This behavior appeared more important for load levels of 17 and 18 kN than for higher load levels of 20 and 22 kN, although the slopes of the curves in Fig. 6 appear more or less the same. This probably account for the fact that fatigue failure occurs faster at higher load levels because cyclic strain amplitude are higher (thus cumulative strain increases faster), limiting the extent to which this apparent cyclic hardening occur.

It is possible that this apparent cyclic hardening behavior is caused by local rearrangements of carbon fiber under the action of the cyclic compressive loads. In this case, fibers initially at an approximate ±45° orientation in the cylindrical specimens would progressively rotate to accommodate for the cumulative strain, which would cause the polymer matrix to be progressively compressed as well as neighboring fibers to get closer to each other. This cumulative strain in a restricted plane strain state results in a progressive increase in stiffness. At a certain level of cumulative strain (and local rotation of fibers), the fibers and matrix would reach the maximum level of rearrangements, leading to rapid increase in stiffness, interfiber contact and eventually interfiber damage, namely by microbuckling. Within the scope and means of this study, it is not possible to confirm whether this cascade of events is effectively taking place. However, it is possible to confirm whether microbuckling of fibers can be observed in the fatigued specimens after failure at locations far from the final fatigue failure site (several mm from the latter), i.e., in the general, non-concentrated cyclic deformation region. SEM observations were made to assess the presence of fiber microbuckling far from the high cumulative strain region. An example of microbuckling of fibers observed several mm from the final fatigue failure region is shown in Fig. 7. This figure demonstrates that at sites where fatigue failure did not occur, i.e., representative of earlier fatigue life, microbuckling occurred. This microbuckling of fibers is caused by their progressive rotation leading to compression stresses along fiber direction due to their confinement (plane strain). Although it cannot be considered as a confirmation of this proposed origin of stiffness increase (cyclic hardening), observation of this phenomenon is in agreement with this proposition.

The hysteresis loops for each load conditions were also analyzed to obtain the cyclic strain amplitude as a function of the number of cycles. Figure 8 illustrates the cyclic strain amplitude evolution in the fatigued specimens. The curves is this figure show three phases: a first stabilization phase during which the load-position cycles became stable; a second phase during most of the fatigue life showing a slightly negative constant strain amplitude rate; and a final

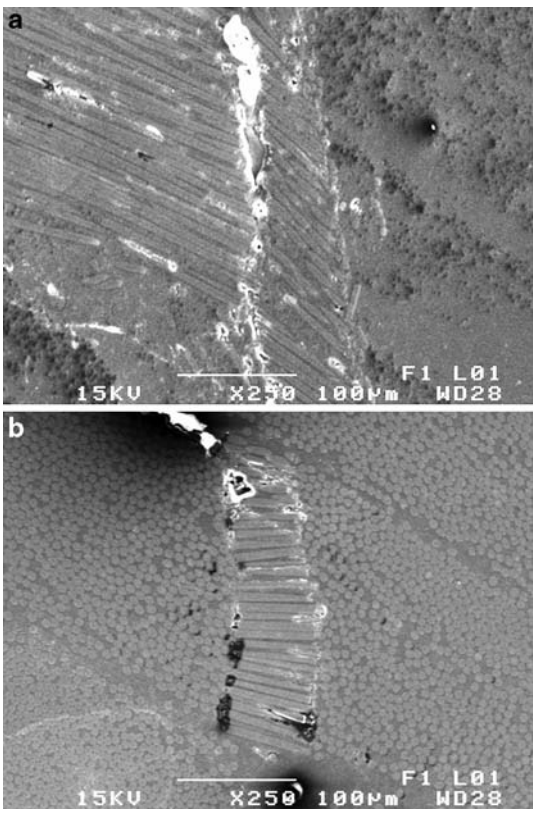

Fig. 7 SEM micrographs of fibers damaged by microbuckling for: (**a**) 18 kN and (**b**) 22 kN

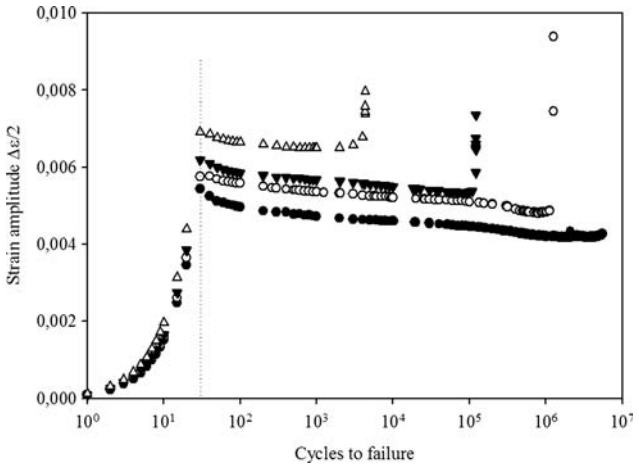

Fig. 8 Strain amplitude as a function of number of cycles to failure for 17 kN (●), 18 kN (○), 20 kN (▼) and 22 kN(△). Line represents cycle 30 where test was stabilized

third phase during which the cyclic strain amplitude increased suddenly until fatigue failure occurred. The slightly negative constant strain amplitude rate in the second phase indicates a weak but significant decrease in total strain amplitude as the number of cycle increases. This observation is in agreement with the observed increase in stiffness during fatigue life: in constant load conditions, an increase in stiffness results in a reduction in deformation. The constant strain amplitude rate obtained in each loading condition as well as the corresponding decrease in cyclic strain amplitude during this second phase are also reported in Table 3. As shown in this table, both the decrease in cyclic strain amplitude and the constant strain amplitude rate steadily decreases when changing from maximum fatigue load of 17–22 kN. This observation that strain amplitude decreases more and faster at lower fatigue loads suggests that the increase in stiffness during fatigue cycling, or cyclic hardening, is more important at lower fatigue loads, in agreement with the extent to which relative stiffness increases depending on the maximum load level (Fig. 6). These strain amplitude related values indicate that fatigue failure occurs faster at higher load levels only because strain amplitude are higher, and therefore cumulative strain increases faster, and also that the mechanisms that lead to the increases in stiffness are independent from those that lead to final failure, since they occur less and slower at higher load levels.

Fatigue of THP stems: Conditions for the fatigue testing of the CF/PA12 composite femoral stems are summarized in Table 4. All specimens were ended after a fatigue life of 10×10^6 cycles, showing their long durability and mechanical reliability. Further analysis of the fatigue data in Fig. 9 revealed that the relative stiffness as a function of the cycles to failure slightly increased as expected, due to

Table 4 Test conditions for compression fatigue testing of CF/PA12 femoral stems

Specimen	Frequency (Hz)	Offset angle (°)	Amplitude (N)	Mean level (N)	Maximum load (N)
PTH 1					
PTH 2	10	11	1000	–1300	2300
PTH 3					

the same apparent cyclic hardening behavior observed for fatigued cylindrical specimens. As shown in this figure, the relative stiffness of the THP stems progressively increases from 1.0 to approximately 1.2 upon cyclic loading, in agreement with increases noted for fatigued cylindrical specimens (Fig. 6). In this case however stiffness was normalized using stiffness of cycle 100 because load cycles took more time to stabilize.

In order to further correlate the fatigue behavior of the fatigued cylindrical specimens to that of the THP stems, hysteresis loops for relevant cycles are reported in Fig. 10. The evolution of the hysteresis loops upon cyclic loading is very similar to that observed for fatigued cylindrical specimens at lower load levels (our case for THP stem testing); surface of hysteresis loops is larger initially, but progressively stabilized as the number of cycles increased as a result of the (very) low loads levels employed. This observation is in agreement with the fact that THP stems in the fatigue load conditions used did not fail after 10×10^6 cycles. It indicates that not only did they not fail, but their cumulative deformation did not lead them to be substantially damaged. This observation is in agreement with the lack of evidence of fatigue damage found from SEM.

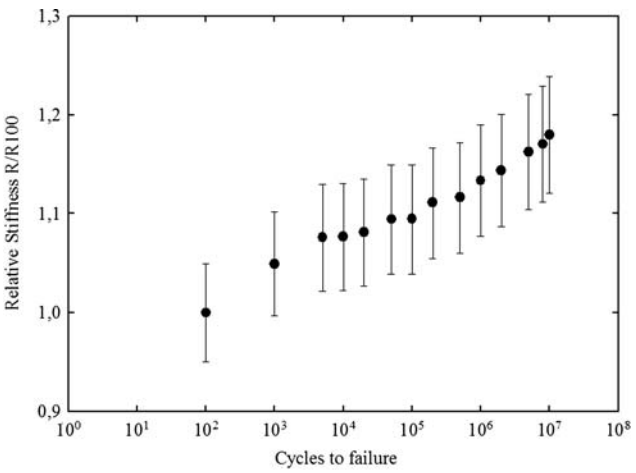

Fig. 9 Relative stiffness as a function of cycles to failure for THP stem. Error bars represent ±5% standard error

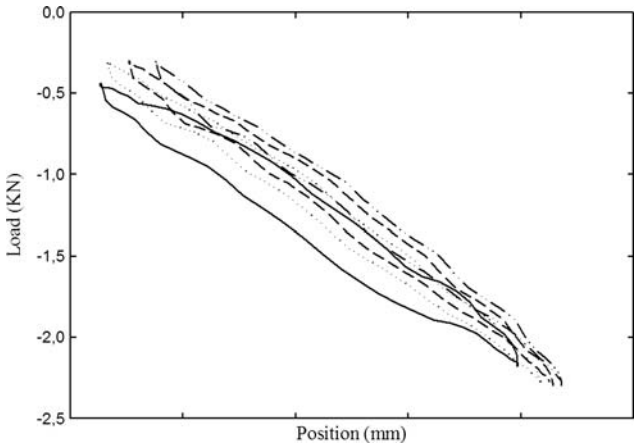

Fig. 10 Evolution of hysteresis loops for a THP stem for cycle 100, 10^5, 10^6 and 10×10^6

While all results found in literature recently include a modulus variation in their design, generally too high in value and very limited in range, none of the designs mentioned previously address the need for a match of the bone modulus, bone density and bone structure for the stem. De Santis et al. measured tensile properties that were uniform along the stem but considerably too high to match bone properties and in bending, again values were far from the cortical bone range. Adam et al. presented an anatomically shaped carbon–carbon hip stem but their clinical results show a high incidence of early aseptic loosening due to the lack of a hydroxyapatite coating or proximal macrotexturing. As for Akay and Aslan, their numerical and experimental study concerned a cemented CF/PEEK composite hip prosthesis, while this femoral stem is non-cemented. Simoes et al. also developed a composite femoral prosthesis; however they chose to combine a flexible outer layer with a metal core, which significantly increases their overall mechanical properties. Finally, none of the above have demonstrated the long term properties of their designs with fatigue testing. This study demonstrated just that; a polymer composite femoral stem with bone-matching properties that would eliminate stress shielding and excellent fatigue results that show potential for an increased life span.

Since CF/PA12 composites have excellent mechanical performance and can be produced with great versatility in complex shapes with tailored properties, their static and dynamic mechanical behavior can be adjusted to be quite close to those of cortical femoral bone. This combination of bone-matching short-term properties and excellent fatigue performance, coupled with the fact that they are chemically inert and potentially biocompatible [13] makes them valuable materials in orthopedic applications such as the hip prosthesis and a the potential to reduce stress shielding and in the long run prevent bone resorption.

Summary and conclusion

The mechanical properties of the CF/PA12 composite were analyzed both in static and dynamic tests. The CF/PA12 cylinders were subjected to a variety of mechanical tests in order to obtain a detailed characterization of the material and how it behaved both in short and long terms. Short terms mechanical properties were shown to be very similar to cortical bone's properties. Fatigue testing revealed that the composite-made stems have excellent fatigue resistance, indicating fatigue life at load levels recommended by ISO standards for testing THP stems exceeding by far the normal life expectancy from these stems of 10×10^6 cycles. In fact, fatigue failure at load levels also 6 times higher than load levels recommended occurred at 5×10^6 to 10×10^6 cycles. Monitoring of cyclic strain amplitude and stiffness evolution during fatigue testing revealed that an apparent cyclic hardening occurred upon cycling, which was more important at lower load levels. In the load level range employed, fatigue damage was related to cumulative strain and local rotation of carbon fibers, as matrix and interfiber damage and fiber microbuckling.

Bone-matching properties of this composite-made THP and its excellent fatigue performance by far surpassing required fatigue life make PA12/CF candidate material of choice for orthopedic devices such as total hip prostheses and might offer a long term solution to stress shielding and bone resorption.

Acknowledgments The collaboration of Terray Corporation for financial participation and for providing materials as well as the financial support of project by NSERC (STP 306867-04) and the National Research Council of Canada are gratefully acknowledged.

References

1. S. KURTZ, E. LAU, K. ZHAO, F. MOWAT, K. ONG, and M. HALPERN, in 73rd Annual Meeting of the American Academy of Orthopaedic Surgeons (Chicago, IL, 2006)
2. D. TAYLOR, C. MARTIN, B. CORNELIS and M. E. B. JONES, *J. Eng. Med.* **207**(2) (1993) 121
3. H. BOUGHERARA, M. N. BUREAU, M. CAMPBELL, A. VADEAN and L'H. YAHIA, *J. Biomed. Mater. Res. A.* **82A**(1) (2007) 27
4. A. REINHARDT, S. G. ADVANI, M. H. SANTARE and F. MILLER, *J. Compos. Mater.* **33**(9) (1999) 853
5. J. A. SIMOES and A. T. MARQUES, *Comp. Sci. Tech.* **60** (2000) 559
6. J. A. SIMOES and A. T. MARQUES, *Compos. Part A* **32** (2001) 655
7. J. A. SIMOES and A. T. MARQUES, *Mater. Des.* **26** (2005) 391
8. F. K. CHANG, J. L. PEREZ and J. A. DAVIDSON, *J. Biomed. Mater. Res.* **24**(7) (1990) 873
9. R. DE SANTIS, L. AMBROSIO and L. NICOLAIS, *J. Inorg. Biochem.* **79**(1–4) (2000) 97
10. F. ADAM, D. S. HAMMER, S. PFAUTSCH and K. WESTERMANN, *J. Arthroplasty* **17**(2) (2002) 217

11. M. AKAY and N. ASLAN, *J. Biomed. Mater. Res.* **31** (1996) 167
12. J. R. BRITTON, C. G. C. LYONS and P. J. PRENDERGAST, *Strain* **40** (2004) 193
13. J.-G. LEGOUX, F. CHELLAT, R. LIMA, B. MARPLE, M. N. BUREAU, H. SHEN and G. A. CANDELIERE, *J. Thermal Spray Technol.* **15**(4) (2006) 629
14. K. CHOI and S. A. GOLDSTEIN, *J. Biomech.* **25**(12) (1992) 1371
15. American Society for Testing and Materials, "ASTM D348-00", Standard Test Methods for Rigid Tubes Used for Electrical Insulation
16. American Society for Testing and Materials, "ASTM D790-03", Standard Test Methods for Flexural Properties of Unreinforced and Reinforced Plastics and Electrical Insulating Materials p. 6
17. American Society for Testing and Materials, "ASTM E2207–02", Standard Practice for Strain-Controlled Axial-Torsional Fatigue Testing with Thin-walled Tubular Specimens
18. O. H. BASQUIN, in "Proceedings of the American Society for Testing and Materials", Vol 10 (1910)
19. International Standard Organization, "ISO7206–4", Implants for Surgery-Partial and Total Hip Joint Prostheses-Part 4: Determination of Endurance Properties of Stemmed Femoral Components
20. American Society for Testing and Materials, "ASTM F1612–95", Standard Practice For Cyclic Fatigue Testing of Metallic Stemmed Hip Arthroplasty Femoral Components with Torsion
21. M. N. BUREAU and J. DENAULT, *Comp. Sci. Tech.* **64** (2004) 1785
22. D. C. WIRTZ, N. SCHIFFERS, T. PANDORF, K. RADERMACHER, D. WEICHERT and R. FORST, *J. Biomech.* **33** (2000) 1325
23. D. T. REILLY and A. H. BURSTEIN, *J. Biomech.* **8**(6) (1975) 393
24. D. T. REILLY, A. H. BURSTEIN and V. H. FRANKEL, *J. Biomech.* **7**(3) (1974) 271
25. S. M. SNYDER and E. SCHNEIDER, *J. Orthop. Res.* **9** (1991) 422
26. H. B. SKINNER, *Orthopedics* **14**(3) (1991) 323
27. G. BERGMANN, F. GRAICHEN and A. ROHLMANN, *J. Biomech.* **26**(8) (1993) 969
28. American Society for Testing and Materials, "ASTM F1440–92", Standard Practice for Cyclic Fatigue Testing of Metallic Stemmed Hip Arthroplasty Femoral Components Without Torsion